MICROBIOLOGY

RESEARCH ARTICLE

Sarwar *et al.*, *Microbiology* 2020;166:867–879

DOI 10.1099/mic.0.000943

MICROBIOLOGY SOCIETY

MifS, a DctB family histidine kinase, is a specific regulator of α-ketoglutarate response in *Pseudomonas aeruginosa* PAO1

Zaara Sarwar[1,*], Michael X. Wang[2]†, Benjamin R. Lundgren[2] and Christopher T. Nomura[2,3,*]

Abstract

The C5-dicarboxylate α-ketoglutarate (α-KG) is a preferred nutrient source for the opportunistic pathogen *Pseudomonas aeruginosa*. However, very little is known about how *P. aeruginosa* detects and responds to α-KG in the environment. Our laboratory has previously shown that the MifS/MifR two-component signal transduction system regulates α-KG assimilation in *P. aeruginosa* PAO1. In an effort to better understand how this bacterium detects α-KG, we characterized the MifS sensor histidine kinase. In this study we show that although MifS is a homologue of the C4-dicarboxylate sensor DctB, it specifically responds to the C5-dicarboxylate α-KG. MifS activity increased >10-fold in the presence of α-KG, while the related C5-dicarboxylate glutarate caused only a 2-fold increase in activity. All other dicarboxylates tested did not show any significant effect on MifS activity. Homology modelling of the MifS sensor domain revealed a substrate binding pocket for α-KG. Using protein modelling and mutational analysis, we identified nine residues that are important for α-KG response, including one residue that determines the substrate specificity of MifS. Further, we found that MifS has a novel cytoplasmic linker domain that is required for α-KG response and is probably involved in signal transduction from the sensor domain to the cytoplasmic transmitter domain. Until this study, DctB family histidine kinases were known to only respond to C4-dicarboxylates. Our work shows that MifS is a novel member of the DctB family histidine kinase that specifically responds to α-KG.

INTRODUCTION

The opportunistic pathogen *Pseudomonas aeruginosa* is well known for its metabolic versatility. It has the ability to assimilate a diverse array of organic molecules for energy, allowing it not only to survive but thrive in harsh environmental conditions. Dicarboxylates, including citric acid cycle intermediates, are one of its preferred nutrient sources [1, 2]. We have previously shown that *P. aeruginosa* PAO1 can survive with C5-dicarboxylate α-ketoglutarate (α-KG) as the sole carbon source [3]. In addition to being an important intermediate of the citric acid cycle, α-KG plays an important role in the detoxification of reactive oxygen species [4, 5] and is required for virulence by several pathogenic bacteria [6, 7]. Hence it is not surprising that bacteria would require signalling pathways to monitor α-KG levels in their environment. However, not much is known about how bacterial cells detect and respond to changing α-KG levels in their environment.

Previous work in our laboratory identified and characterized the *PA5530* gene, encoding an α-KG symporter, that is required for transport of α-KG into the cell [3]. We showed that expression of the *PA5530* gene is activated in the presence of α-KG by the MifS/MifR two-component signal transduction system (TCS) in *P. aeruginosa* PAO1 [3]. TCSs are widely used by bacteria to sense and respond to changes in their environment [8, 9]. A TCS is typically composed of a sensor histidine kinase and a response regulator. Upon binding its ligand, the histidine kinase is autophosphorylated at a conserved histidine residue. The phosphate is then transferred to a conserved aspartate residue on the response regulator, thus activating it. The activated response regulator then goes

Received 27 February 2020; Accepted 27 May 2020; Published 17 June 2020

Author affiliations: [1]Department of Biology, The College of New Jersey, Ewing, New Jersey, USA; [2]Department of Chemistry, The State University of New York, College of Environmental Science and Forestry, Syracuse, New York, USA; [3]Center for Applied Microbiology, The State University of New York, College of Environmental Science and Forestry, Syracuse, New York, USA.

***Correspondence:** Christopher T. Nomura, ctnomura@esf.edu; Zaara Sarwar, sarwarz@tcnj.edu

Keywords: MifS; two-component signal transduction systems; sensor histidine kinase; α-ketoglutarate; dicarboxylate sensor; *Pseudomonas aeruginosa*.

Abbreviations: Amp, ampicillin; CA, catalytic and ATP binding subdomain; COG, clusters of orthologous groups; DHp, dimerization and histidine phosphorylation subdomain; Gm, gentamicin; α-KG, α-ketoglutarate; LB, Lennox broth; MU, Miller units; PDC, PhoQ-DcuS-CitA; TCS, two component signal transduction system.

†Present address: Biomedical Sciences Graduate Program, University of California, San Diego, California, USA.

Two supplementary figures are available with the online version of this article.

on to modulate cellular activity in response to the signal. Several dicarboxylate-sensing TCSs have been identified and characterized in bacteria [10–12]. However, only two TCSs, including MifS/MifR, have so far been shown to be involved in α-KG response [3, 7].

In this study, we describe the structural and functional analysis of the MifS sensor domain, the only α-KG sensor histidine kinase to be characterized to date. Our work shows that MifS is a specific sensor for the C5-dicarboxylate α-KG. Sequence analysis and protein modelling revealed that the periplasmic sensor domain of MifS has a mixed α/β PDC (PhoQ-DcuS-CitA) fold typical of other dicarboxylate sensors [10, 12–14]. Using our model of the MifS sensor domain and mutational analysis, we identified residues in the MifS sensor domain that are required for α-KG response. We have also identified a novel cytoplasmic linker domain in MifS that is required for signal transduction and appears to be conserved in other DctB family histidine kinases.

METHODS

Bacterial strains, media and growth conditions

The bacterial strains used in this study are listed in Table 1. Bacteria were grown in Lennox broth (LB). Solid bacteriological media was prepared with the addition of agar (BD Difco) at 15 g l^{-1}. Liquid cultures were grown at 30 °C with shaking at 250 r.p.m. and cultures on solid bacteriological media were grown by incubation at 37 °C. When required, the antibiotics ampicillin (Amp, 100 μg ml^{-1}) or gentamicin (Gm, 10 μg ml^{-1}) were added to culture media to maintain plasmids.

Molecular biology methods

All of the plasmids used in this study are listed in Table 1. Plasmid DNA was purified using the EZNA Plasmid DNA Mini Kit I (Omega Bio-tek). The plasmid pBRL566 [3] expressing the *mifSmifR* genes from the trc promoter and plasmid pBRL485 [3] expressing the *Escherichia coli lacZ* gene from the *PA5530* promoter were used in this study. Mutations were inserted into the *mifS* gene harboured in pBRL566 using the QuikChange Site-Directed Mutagenesis kit (Agilent Technologies) or the Q5 Site-Directed Mutagenesis kit (New England BioLabs) as per the manufacturers' protocols. All oligonucleotides used for site-directed mutagenesis are provided in Table 2 and were designed using QuikChange Primer Design for the QuickChange Site-Directed Mutagenesis kit or NEBaseChanger for the Q5 Site-Directed Mutagenesis kit. The sequences of plasmids containing mutations in *mifS* were verified by Sanger sequencing (Genewiz, NJ, USA).

LacZ-reporter assays

E. coli Top10 cells harbouring the pBRL485 plasmid and either the pBRL566 plasmid or a plasmid carrying a *mifS* mutant gene (Table 1) were grown in LB media at 30 °C with shaking at 250 r.p.m. to an optical density at 600 nm (OD_{600}) value of 0.3. Cells were then induced with various dicarboxylates at a final concentration of 20 mM and allowed to grow for an additional 60 min post-induction. Each mutation and/or condition was tested in triplicate (n=3). β-galactosidase (LacZ) activity was measured using the Miller assay as described previously [15, 16].

Protein modelling and ligand docking

The SWISS-MODEL homology modelling server [17] was used to model the MifS periplasmic sensor domain using DctB of *Vibrio cholerae* (PDB ID: 3by9) [10] as a template. AutoDock Vina version 1.1.2 was used for all ligand docking in this study [18]. Default values for docking parameters were used. The lowest energy conformation was chosen for further analysis. To verify the accuracy of ligand docking via AutoDock Vina, succinate was docked into the DctB binding pocket. We found that AutoDock Vina was able to generate the correct binding position as observed by protein crystallography (data not shown). Hydrogen bonds between substrate and binding pocket were predicted using PyMOL version 2.3.2 [19]. Structural alignment of the MifS binding pocket and *V. cholerae* DctB binding pocket was performed using PyMOL version 2.3.2 [19].

RESULTS

MifS is an HPK4 family histidine kinase

Histidine kinases are typically composed of a periplasmic/extracellular sensor domain and a cytoplasmic transmitter domain [20]. The sensor domains of histidine kinases differ widely in sequence from one another due to the great range of signals they detect [9, 21]. Sequence analysis showed that MifS is a histidine kinase with a periplasmic sensor domain flanked by two transmembrane helices, TMH1 and TMH2 (Fig. 1a). TMH2 is followed by a 42 residue long cytoplasmic segment linking the sensor and transmitter domains. The transmitter domain of histidine kinases is highly conserved in sequence and further subdivided into the dimerization and histidine phosphorylation subdomain (DHp), and the catalytic and ATP binding subdomain (CA) [20]. The DHp is characterized by the conserved sequence motif known as the H-box that contains the phospho-accepting His residue [22]. The CA typically contains the N-, F-, D- and G-boxes, all of which are required for ATP hydrolysis [22]. Based on variations in these signature sequence motifs found in the transmitter domain, histidine kinases are grouped into 14 different families [22–24]. We analysed the sequence of MifS and determined that it belongs to the HPK4 family of histidine kinases. MifS has all the major HPK4 family sequence features, such as the AHE motif in the H-box, the DxGxG and PFxTTK motif in the D-box, and the GxGxGx motif in the G-box (Fig. 1b) [22]. The original classification of histidine kinases by Grebe and Stock [22] included two DctB sequences, both of which were categorized in the HPK4 family. Since then, the number of available histidine kinase sequences has increased immensely. Therefore, we decided to check if di-carboxylate binding histidine kinases such as MifS and DctB show any special features to distinguish them from other HPK4 family members. A BLAST search revealed that MifS belongs to the clusters of orthologous groups (COG)

Table 1. Bacterial strains and plasmids used in this study

Bacterial strains, plasmids	Relevant characteristics	Reference or source
Strains		
Escherichia coli Top10	F- *mcrA Δ(mrr-hsdRMS-mcrBC) φ80lacZΔM15 ΔlacX74 nupG recA1*	Invitrogen
E. coli NEB5-alpha	*fhuA2 Δ(argF-lacZ)U169 phoA glnV44 Φ80 Δ(lacZ)M15 gyrA96 recA1 relA1 endA1 thi-1 hsdR17*	New England Biolabs
Plasmids		
pTrc99a	Expression plasmid; Amp^r	Pharmacia
pBBR1MCS-5	Broad host-range plasmid; Gm^r	[55]
Δ*Plac*-pBBR1MCS-5	pBBR1MCS-5 minus *lac* promoter; Gm^r	[46]
pBRL485	*PA5530-lacZ* in Δ*Plac*-pBBR1MCS-5	[3]
pBRL566	*mifSR* operon in pTrc99a; Amp^r	[3]
pZS428	*mif*SR135A-*mifR* operon in pTrc99a; Amp^r	This study
pZS429	*mif*SS156A-*mifR* operon in pTrc99a; Amp^r	This study
pZS435	*mif*SH372A-*mifR* operon in pTrc99a; Amp^r	This study
pZS487	*mif*SL336A-*mifR* operon in pTrc99a; Amp^r	This study
pZS488	*mif*SE337A-*mifR* operon in pTrc99a; Amp^r	This study
pZS489	*mif*S^V340A-*mifR* operon in pTrc99a; Amp^r	This study
pZS490	*mif*SE341A-*mifR* operon in pTrc99a; Amp^r	This study
pZS491	*mif*SR338A-*mifR* operon in pTrc99a; Amp^r	This study
pZS493	*mif*SL339A-*mifR* operon in pTrc99a; Amp^r	This study
pMW03	*mif*SY132A-*mifR* operon in pTrc99a; Amp^r	This study
pMW04	*mif*SY132F-*mifR* operon in pTrc99a; Amp^r	This study
pMW06	*mif*SY137A-*mifR* operon in pTrc99a; Amp^r	This study
pMW07	*mif*SK181A-*mifR* operon in pTrc99a; Amp^r	This study
pMW11	*mif*SY127A-*mifR* operon in pTrc99a; Amp^r	This study
pMW14	*mif*SE107A-*mifR* operon in pTrc99a; Amp^r	This study
pMW15	*mif*SF162A-*mifR* operon in pTrc99a; Amp^r	This study
pMW16	*mif*SF162Y-*mifR* operon in pTrc99a; Amp^r	This study
pMW20	*mif*SV154S-*mifR* operon in pTrc99a; Amp^r	This study
pMW21	*mif*SE107Y-*mifR* operon in pTrc99a; Amp^r	This study
pMW22	*mif*SV154S/F162Y-*mifR* operon in pTrc99a; Amp^r	This study
pMW23	*mif*SY137F-*mifR* operon in pTrc99a; Amp^r	This study
pMW24	*mif*SY127F-*mifR* operon in pTrc99a; Amp^r	This study
pMW26	*mif*SN483A-*mifR* operon in pTrc99a; Amp^r	This study
pMW29	*mif*SD517A-*mifR* operon in pTrc99a; Amp^r	This study
pMW32	*mif*SΔ340–346-*mifR* operon in pTrc99a; Amp^r	This study

Table 2. Oligonucleotides used in this study

Oligonucleotide	Sequence
ZS428.f	GGCGGAAATAGGGAGCGAAACCGTAGTTGTGGCC
ZS428.r	GGCCACAACTACGGTTTCGCTCCCTATTTCCGCC
ZS429.f	ACCGGGAATCCCGGCGATCACCCCGACC
ZS429.r	GGTCGGGGTGATCGCCGGGATTCCCGGT
ZS435.f	GCTGGTTGATCTCAGCGGCCAGGGCTGCCG
ZS435.r	CGGCAGCCCTGGCCGCTGAGATCAACCAGC
ZS455.f	CGGCAGGTTCCAGGCGCTCGCCGCCACG
ZS455.r	CGTGGCGGCGAGCGCCTGGAACCTGCCG
ZS456.f	TCGGCAGGTTCCACTCGCTCGCCGCCACG
ZS456.r	CGTGGCGGCGAGCGAGTGGAACCTGCCGA
ZS457.f	ATAGGGACGGAAACCGGCGTTGTGGCCCACGTAG
ZS457.r	CTACGTGGGCCACAACGCCGGTTTCCGTCCCTAT
ZS459.f	GGACGGAAACCGAAGTTGTGGCCCACGTAG
ZS459.r	CTACGTGGGCCACAACTTCGGTTTCCGTCC
ZS460.f	GAAATAGGGACGGAAACCCATGTTGTGGCCCACGTAGCT
ZS460.r	AGCTACGTGGGCCACAACATGGGTTTCCGTCCCTATTTC
ZS474.f	CGAGCAGCGCGAAGCCGACCTGCG
ZS474.r	ACCAGGCGCTCCAGCTCC
ZS475.f	CGAGCAGCGCGCAGCCGACCTGC
ZS475.r	ACCAGGCGCTCCAGCTCC
ZS476.f	GAGCGTCGCCGCTAACGGCGGCG
ZS476.r	AGCACCCAGTCGCCGCCA
ZS477.f	GGTGCTGGTCGCTCTGCTGCGCAACG
ZS477.r	TGTTCCAGGCGGATCGCG
ZS482.f	CTGCTGCGTACCGCGCAGGAC
ZS482.r	GTCGGCGGTGCGCTGCTC
ZS483.f	CTGCGTACCGCGCAGGAC
ZS483.r	CAGGCGCTCCAGCTCCTC
MW02.f	TTTCCGTCCCGCTTTCCGCCAGACCATC
MW02.r	CCGTAGTTGTGGCCCACG
MW03.f	AATCGTGGTCGCTCTGGAGTTTCCCGATCTGGAACGG
MW03.r	GCGCCCAGGAAGCTGCCG
MW06.f	GACCATCGCCGCTGGCTCCGGAC
MW06.r	TGGCGGAAATAGGGACGG
MW07.f	GCCGACCAGCGCTGTGGGCCACAAC
MW07.r	AGGTTCCAGTTGCTCGCC
MW10.f	TCCACCCTGGCGCTGCTCGACC
MW10.r	GGAGCGGGCGGCCAGGTT
MW11.f	TCCCGGTTATGCCCTGTCCCACG
MW11.r	ATCCCGCTGATCACCCCG
MW12.f	CCCGGTTATTACCTGTCCCAC
MW12.r	AATCCCGCTGATCACCCC
MW15.f	CTACGGTTTCTATCCCTATTTCCGCCAGAC
MW15.r	TTGTGGCCCACGTAGCTG
MW16.f	TGCGGTCGGGAGTATCAGCGGGATTC
MW16.r	TAGAAACGTCCGGAGCCT
MW17.f	CTCCACCCTGTATCTGCTCGACCGTACC
MW17.r	GAGCGGGCGGCCAGGTTG
MW18.f	CGGTCGGGAGTATCAGCGGGATTC
MW18.r	CATAGAAACGTCCGGAGCC
MW19.f	TTTCCGTCCCTTTTTCCGCCAGAC
MW19.r	CCGTAGTTGTGGCCCACG
MW20.f	GCCGACCAGCTTTGTGGGCCACA
MW20.r	AGGTTCCAGTTGCTCGCC

family COG4191 that represents the 'Signal transduction histidine kinase regulating C4-dicarboxylate transport system' family of proteins consisting of ~22000 histidine kinases from 3500 different species [25, 26]. Alignment of MifS with the COG4191 consensus sequence showed that, in addition to all the signature features of the HPK4 family, MifS and DctB homologues possess two unique features (Fig. 1b). DctB family histidine kinases, including MifS, have an invariable N as the third residue following the phosphor-accepting histidine followed by a conserved N/Q. MifS and DctB homologues also have a highly conserved IRLE motif in the N-box preceding the first N that is not present in other HPK4 members.

MifS sequence has characteristic motifs of conserved transmitter domain

We have previously shown that the MifS/MifR TCS regulates expression of the *PA5530* gene encoding an α-KG symporter in *P. aeruginosa* PAO1 [3]. Our work and that of others has also shown that both the *mifS* and *mifR* genes are required for growth in the presence of α-KG [3, 27]. To experimentally verify that MifS acts as a histidine kinase *in vivo*, we made mutations of the predicted phospho-accepting His372 in the DHp subdomain, along with two residues in the CA subdomain predicted to be required for ATPase activity, namely, the N-box Asn483 and the D-box Asp517. We heterologously expressed the wild-type *mifS* gene or a variant containing the H372A, N483A, or D517A mutation from the trc promoter in *E. coli* Top10 cells harbouring a constitutively expressed wild-type *mifR* gene and the P_{PA5530}::*lacZ* reporter (~1000 bp 5′ regulatory region upstream of the *PA5530* gene fused to the *lacZ* gene of *E. coli* [3]). *E. coli* has no homologues of MifS or MifR, and so to study the function of the MifS protein we chose to use *E. coli* as a heterologous host in order

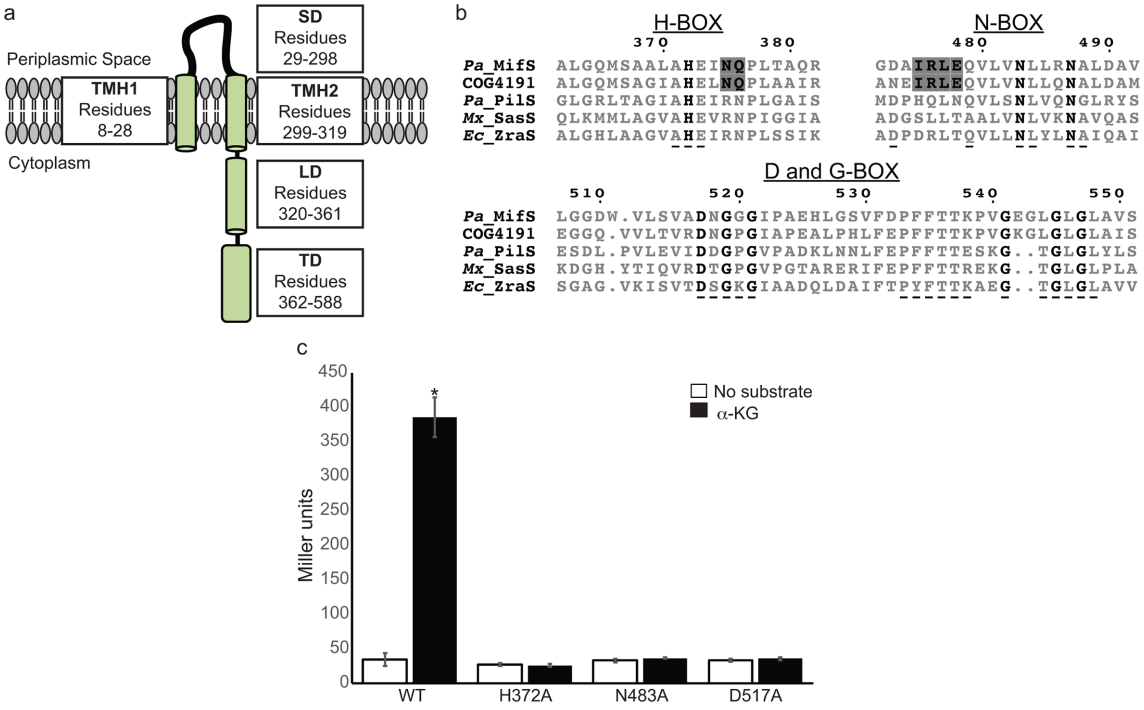

Fig. 1. MifS is a DctB family transmembrane histidine kinase. (a) Domain architecture of MifS showing a periplasmic sensor domain (SD) flanked by two transmembrane helices (TMH1 and TMH2). TMH2 is followed by a cytoplasmic linker domain (LD) attached to a cytoplasmic transmitter domain (TD). (b) Alignment of the transmitter domain sequences of *Pseudomonas aeruginosa* MifS, COG4191 consensus sequence representing the DctB family of sensor histidine kinases, and HPK4 family histidine kinases from *P. aeruginosa* (*Pa*), *Myxococcus xanthus* (*Mx*) and *Escherichia coli* (*Ec*). The invariant residues of each transmitter domain conserved sequence box are shown in bold type. Conserved HPK4 sequence motifs are indicated with an underscore (_) . Sequence motifs conserved between MifS and DctB COG4191are highlighted in grey. Alignment was generated using CLUSTAL Omega [56] and displayed using ESPript 3.0 [57]. (c) Wild-type MifS, or a MifS variant harbouring a mutation in one of the essential transmitter domain residues (MifSH372A, MifSN483A, or MifSD517A), was expressed in *E. coli* cells harbouring the *mifR* gene and the P_{PA5530}*::lacZ* reporter. Cells were grown in LB media to an optical density at 600 nm (OD_{600}) value of 0.3. They were then challenged with α-KG or no substrate and allowed to grow for an additional 60 min post-induction. Data points represent mean values±the standard deviations (*n*=3). Analysis of variance was performed by using Dunnett's post-hoc test (α value of 0.05) to identify significant differences (*P*<0.0001; marked with an asterisk).

to prevent non-specific activation of *lacZ* expression. When induced with α-KG, cells harbouring the wild-type *mifS* gene showed β-galactosidase (LacZ) activity of 385 MU, while cells expressing MifSH372A, MifSN483A, or MifSD517A exhibited LacZ levels of 26 MU, 36 MU, 35 MU, i.e. ~12-fold lower LacZ activity than cells expressing the wild-type *mifSR* genes (Fig. 1c). This expression was at the same level as that of uninduced cells, which showed LacZ levels of ~34 MU. Thus, each of these mutations rendered MifS inactive, suggesting that H372, N483 and D517 are essential for MifS biological activity. To further verify that the MifS/MifR system was required for expression of the P_{PA5530}*::lacZ* reporter, we found that in the absence of the *mifSmifR* operon there is no LacZ activity from the P_{PA5530}*::lacZ* reporter (Fig. S1, available in the online version of this article).

MifS responds to α-KG with high specificity

Our previous studies revealed that the MifS/MifR TCS regulated *PA5530* expression in response to α-KG [3]. In order to further define the specificity of MifS, we used our P_{PA5530}*::lacZ* reporter fusion to test the activity of MifS in the presence of 13 different dicarboxylates ranging from 3 carbons to 6 carbons in length, including key citric acid cycle intermediates (Fig. 2). In uninduced cells with no substrate present, the activity of the P_{PA5530}*::lacZ* reporter fusion was only 34 MU. In the presence of α-KG, the LacZ levels increased >10-fold to 385 MU, while in the presence of glutarate the increase was only ~2-fold (74 MU). Interestingly, in the presence of the related C5-dicarboxylate glutamate, LacZ levels were 33 MU, similar to that in the absence of any substrate. Furthermore, there was no significant increase of activity over uninduced levels in the presence of any C3-, C4- or C6-dicarboxylates tested. These data suggest that MifS is only active in the presence of the C5-dicarboxylates α-KG and glutarate, with a very strong preference for α-KG.

The periplasmic sensor domain of MifS has an α-KG binding pocket

To understand why MifS responds with high specificity to α-KG, we constructed a model of the MifS sensor domain using the SWISS-MODEL homology modelling server [17]. Analysis of this MifS sensor domain structure showed that the

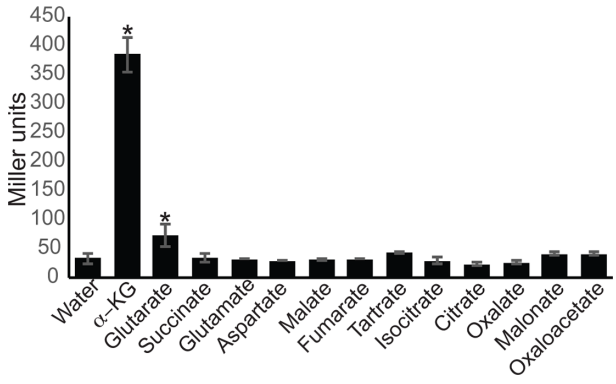

Fig. 2. MifS activity is induced by α-KG. *E. coli* cells harbouring the P_{PA5530}::*lacZ* reporter and the *mifSR* genes were grown in LB media to an OD_{600} value of 0.3 and induced with a panel of dicarboxylates at a final concentration of 20 mM. LacZ expression levels were measured 60 min post-induction. Data points represent mean values±the standard deviations (n=3). Analysis of variance was performed by using Dunnett's post-hoc test (α value of 0.05) to identify significant differences (P<0.0001; marked with an asterisk).

sensor domain is divided into two similar subdomains each with an α/β fold (Fig. 3a). Interestingly, this mixed α/β fold, known as the PDC fold, has been observed in all dicarboxylate sensor histidine kinases characterized to date, including DctB, DcuS and CitA [10, 12, 28]. As is characteristic of PDC domains, the MifS sensor domain starts with a long N-terminal α-helix, α1. The membrane-proximal subdomain is composed of three α-helices (α5–7) packed around a core β-sheet composed of six parallel β-strands. The membrane-distal subdomain is composed of three α-helices (α2–4) that are packed around a core five-stranded parallel β-sheet.

So, how does the MifS sensor domain specifically recognize α-KG? To visualize the molecular interactions involved in the binding of α-KG to MifS, we performed a ligand docking of α-KG to MifS using AutoDock Vina [18]. Our resulting model predicted the binding pocket to be in the distal subdomain of the sensor domain (Fig. 3a). Multiple residues of interest potentially involved in ligand–protein interactions were predicted, specifically Glu107, Tyr127, Tyr132, Arg135, Tyr137, Val154, Ile 155, Ser156, Phe162 and Lys181 (Fig. 3b).

Next, to examine the roles of these residues in α-KG response, we created mutations in the MifS sensor domain and assayed their activity. The MifS mutants were heterologously expressed in *E. coli* Top10 cells expressing wild-type MifR and the P_{PA5530}::*lacZ* reporter. LacZ activity was measured in the presence and absence of α-KG. We first tested residues within the MifS sensor domain that were predicted to be side-chain hydrogen bond donors, namely, Y127A, R135A, Y137A, S156A and K181A (Fig. 3b). When induced with α-KG, LacZ

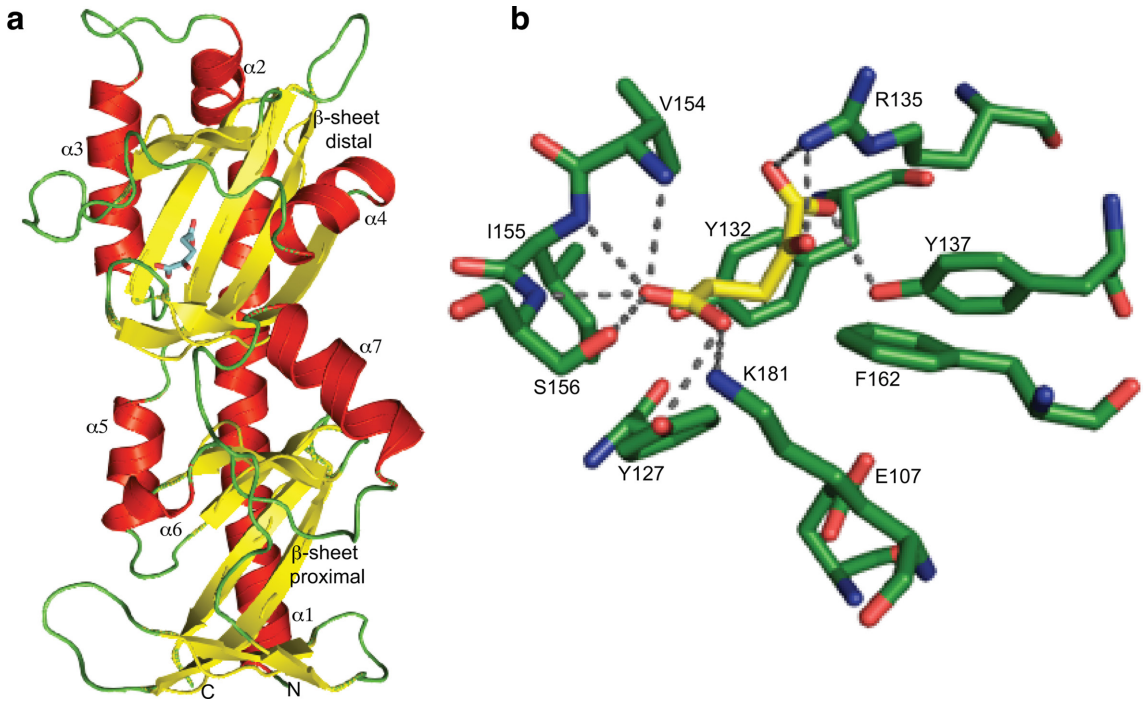

Fig. 3. MifS sensor domain has an α-KG binding pocket. (a) Structural model of the MifS periplasmic sensor domain showing the two mixed α/*β* fold PDC domains, each containing a central *β*-sheet surrounded by three α-helices. The α-KG molecule is shown in blue bound to the distal PDC domain. The homology model of the MifS sensor domain was constructed using the SWISS-MODEL homology server [17]. (b) Model of the MifS binding pocket showing α-KG interacting with binding pocket residues via predicted hydrogen bonds to the side-chains and backbones of the binding pocket residues. α-KG was docked into the MifS sensor domain using AutoDock Vina [18] and protein–ligand hydrogen bonds were predicted using PyMOL [19].

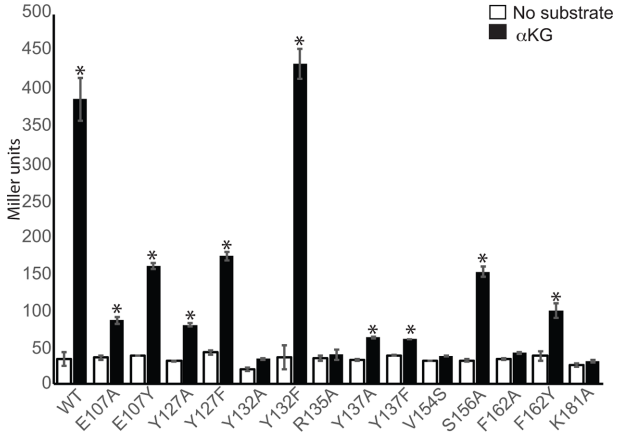

Fig. 4. The MifS sensor domain is required for response to α-KG. Mutations were introduced into the sensor domain of MifS. The wild-type *mifS* gene or one of the mutated *mifS* genes were introduced into *E. coli* cells harbouring the *mifR* gene and the P_{PA5530}::*lacZ* reporter. Cells were grown in LB media to an OD_{600} value of 0.3 and challenged with α-KG (black) or no substrate (white). LacZ expression levels were measured 60 min post-induction. Data points represent mean values±the standard deviations (n=3). Analysis of variance was performed by using Dunnett's post-hoc test (α value of 0.05) to identify significant differences (P<0.0001; marked with an asterisk).

activity in cells expressing wild-type MifS was >10-fold that of uninduced cells (Fig. 4). In cells harbouring the Y137A, Y127A and S156A mutants, LacZ activity in the presence of α-KG was 6-, 5- and 2.5-fold lower than that observed for wild-type MifS, while the R135A and K181A mutants showed no significant activity (Fig. 4). Moreover, LacZ activity for Y127F and Y137F was ~two- and sixfold lower than for wild-type MifS, respectively, suggesting that the hydroxyl group of both Y127 and Y137 is of significant importance, most likely functioning as a hydrogen bond donor during protein–ligand interactions (Fig. 4). These results suggest that Y127, R135, Y137, S156 and K181 are all essential for full MifS biological activity and that these residues likely act as hydrogen bond donors during protein–ligand interactions, agreeing with the predicted hydrogen bonding pattern of our binding pocket model (Fig. 3b).

Our model also shows the presence of a third Tyr residue, Y132, in the binding pocket (Fig. 3b). However, Y132 is not predicted to interact with the substrate through hydrogen bonding. To investigate its role in the binding of α-KG we tested the activity of the Y132A and Y132F mutations. There was no significant P_{PA5530}::*lacZ* expression in the presence of α-KG for the Y132A mutant, while the Y132F mutant showed wild-type level expression (Fig. 4), indicating that either Tyr or Phe at position 132 is sufficient for MifS biological activity. Hence, despite containing a potential hydrogen bond donor, Y132 is not involved in side-chain hydrogen bonding with α-KG. One possible reason for this is that Y132 is most likely involved in hydrophobic interactions, as cells expressing the MifS Y132F mutation had wild-type level activity. Another plausible explanation is the potential for an anion–quadrupole interaction between the aromatic rings of either Tyr or Phe with the conjugated carbonyl of α-KG. These types of interactions with carbonyl groups from glutamate and aspartate with Tyr or Phe residues have been demonstrated previously [29].

Another aromatic residue likely to be part of the α-KG binding pocket was F162. The F162A mutation produced no significant LacZ expression (Fig. 4), suggesting that F162 is required for the biological activity of MifS. Additionally, there was a ~fourfold decrease in activity for the F162Y mutation compared to wild-type MifS (Fig. 4). This suggests that F162 is most likely involved in hydrophobic interactions with the ligand and the addition of a hydroxyl group to F162 disrupts effective protein–ligand interactions.

Two more residues of interest were V154 and E107 of MifS (Fig. 3b). Our protein modelling predicted that V154 of MifS interacts with α-KG via main-chain hydrogen bonding. Interestingly, a V154S mutation showed no significant increase in LacZ activity in the presence of α-KG, suggesting that adding a hydroxyl group to V154 disrupts MifS biological activity (Fig. 4). Our model also shows that the E107 residue is near the binding pocket, but no interaction is predicted with the substrate. Sequence alignment with DctB homologues shows that tyrosine is highly conserved among dicarboxylate sensing HKs, with the glutamate in MifS being the exception (Fig. 5a). α-KG-induced LacZ activity was only 86 and 160 MU for cells containing MifS E107A and E107Y mutations, respectively, i.e. ~4.5- and 2.4-fold lower than for α-KG-induced wild-type MifS (Fig. 4). This suggests that the Glu at position 107 of MifS plays a significant role in α-KG recognition by the MifS sensory domain.

Three further mutations were assayed in residues located adjacent to the predicted binding pocket, namely N120A, N120E and Q144A. None of these mutations showed any significant effect on MifS activity (Fig. S2). This suggests that not all residues in the vicinity of the predicted binding pocket are essential for α-KG response.

The F162Y mutation increases succinate-induced MifS activity

The F162 residue of MifS aligns with a Tyr residue, Y157, in the *V. cholerae* DctB (*Vc*DctB) (Fig. 5a). This Y157 residue of *Vc*DctB is required for succinate binding [[10]]. Since the F162Y mutation disrupts MifS activity significantly (Fig. 4), we wondered whether the F162 residue could play a significant role in the specificity of MifS for α-KG versus succinate. We found that succinate-induced LacZ expression of the F162Y mutant was >twofold higher than succinate-induced expression for wild-type MifS (Fig. 5b). Next, we tested a panel of dicarboxylates on the MifSF162Y mutant, including the C4-dicarboxylates malate and fumarate, both of which are recognized by DctB [10]. Interestingly, no significant activity was observed for any of these C4-dicarboxylates (Fig. 5b). In addition, glutarate-induced LacZ expression of cells containing the F162Y mutation was reduced to half that of the wild-type (Fig. 5b). These results

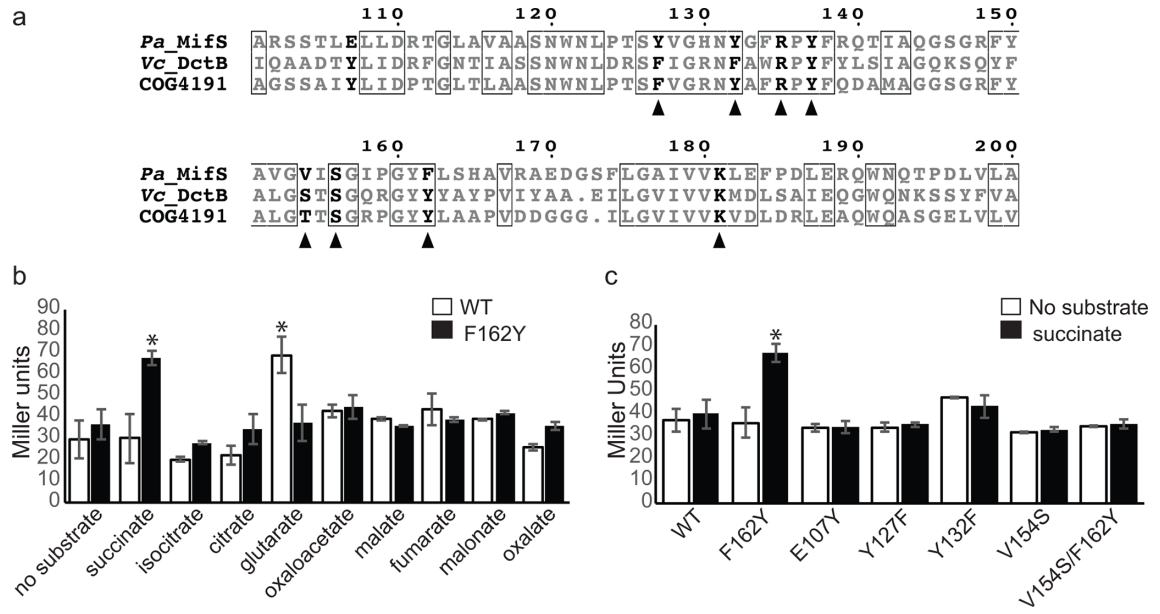

Fig. 5. MifS sensor domain residue Phe162 required for substrate specificity. (a) Alignment of substrate binding pocket sequences of MifS, *Vc*_DctB and COG4191 (DctB family consensus sequence). Residues conserved in all three sequences are shown in boxes. Residues required for α-KG response in MifS are shown in bold. Residues required for succinate binding in *Vc*_DctB are indicated with a triangle. Alignment was generated using CLUSTAL Omega [56] and displayed using ESPript 3.0 [57]. (b) *E. coli* cells harbouring the wild-type *mifS* gene or the *mifSF162Y* gene along with the *mifR* gene and P_{PA5530}::*lacZ* reporter were grown in LB media to an OD_{600} value of 0.3 and induced with a panel of dicarboxylates at a final concentration of 20 mM. (c) Wild-type MifS or a MifS variant with a mutation resembling the *Vc*_DctB binding pocket was expressed in *E. coli* cells harbouring the *mifR* gene and the P_{PA5530}::*lacZ* reporter. Cells were grown in LB media to an OD_{600} value of 0.3 and challenged with succinate or no substrate. LacZ expression levels were measured 60 min post-induction. Data points represent mean values±the standard deviations (n=3). Analysis of variance was performed by using Dunnett's post-hoc test (α value of 0.05) to identify significant differences (P<0.0001; marked with an asterisk).

suggest that the addition of the hydroxyl group via a F162Y mutation within the proposed MifS binding pocket may increase the ability of MifS to recognize succinate while decreasing MifS C5-dicarboxlayte recognition.

Based on these results, we hypothesized that continuing to mutate the MifS binding pocket to more closely resemble the *Vc*DctB binding pocket would continue to increase activity under succinate induction (Fig. 5a). However, contrary to our hypothesis, succinate-induced LacZ expression levels showed no significant increase for any of the other DctB-like mutations in the proposed MifS binding pocket, namely, E107Y, Y127F, Y132F and V154S (Fig. 5c). Interestingly, succinate-induced LacZ activity of the V154S/F162Y double mutant also remained unchanged (Fig. 5c), suggesting that a complicated interaction between residues is required to determine specificity.

Cytoplasmic linker domain required for MifS activity

MifS has a predicted linker domain composed of a 42 residue long peptide, spanning from residue 321 to 362, that links the end of TMH2 and the start of the DHp domain (Fig. 1a). Sequence analysis shows that this linker domain is highly conserved in DctB family histidine kinases with a 21 (3 heptad)-residue insert (Fig. 6a) and includes residues indicated in succinate response in DctB [30]. It is predicted to be α-helical with a high probability of coiled coil formation from residue 332 to 346. Coiled coils are formed when two or more adjacent α-helices are arranged into a super-coiled oligomer [31–33]. A propensity to form coiled coils is predicted by the presence of repeating heptads annotated 'abcdefg' where the residues at positions a and d are conserved hydrophobic residues, typically leucine, required for the interaction of the adjacent helices to adopt the coiled coil structure [34, 35]. To investigate the role of the coiled-coil segment of the MifS linker domain on α-KG response, we decided to analyse one set of predicted heptads starting at residue L336. The residues L336 and L339 were predicted to be at the a and d positions, respectively (Fig. 6b). The L336A and L339A mutations abolished response to α-KG and a V340A mutation showed a twofold reduction in response (Fig. 6c). However, E337A, R338A and E341A mutations did not have any effect on MifS activity (Fig. 6c). We also constructed and tested a deletion mutant spanning from residue 340 to 346 that would disrupt two consecutive heptads. This MifSΔ340–346 mutant showed wild-type level activities in the presence of α-KG. However, in the absence of substrate, the deletion mutant activity was also comparable to that of α-KG induced wild-type MifS (Fig. 6c). Thus, the deletion mutation appears to lead to constitutive activity of MifS.

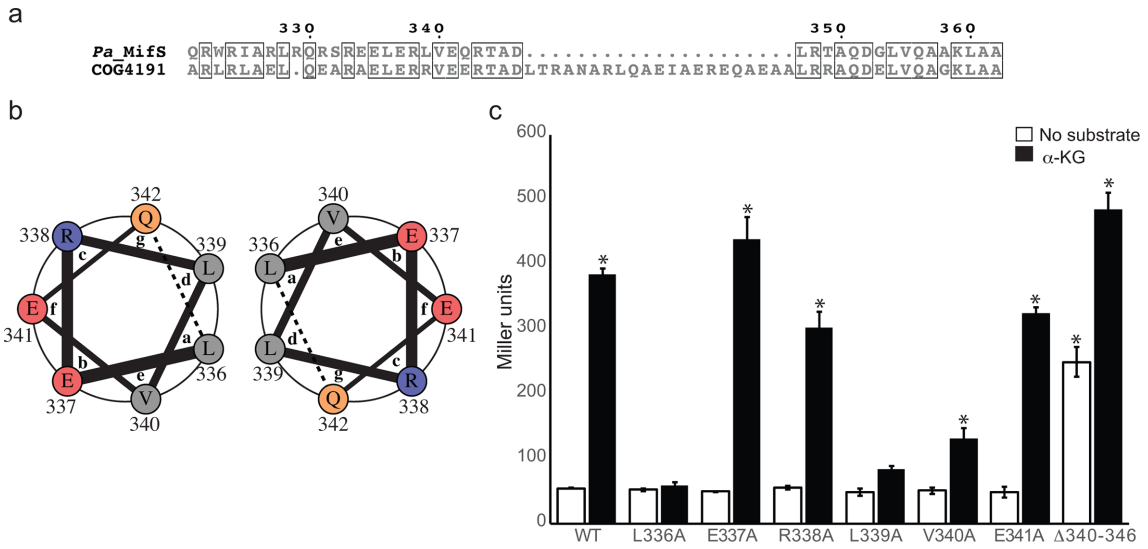

Fig. 6. Linker domain involved in MifS α-KG response. (a) Alignment of cytoplasmic linker domain sequences of MifS and COG4191 (DctB family consensus sequence). Positions with identical residues are boxed. Alignment was generated using CLUSTAL Omega [56] and displayed using ESPript 3.0 [57]. (b) Helical wheel representation of one heptad of the linker domain spanning from residue 336 to residue 342. The interactions between the a position L336 and the d position L339 of two adjacent helices are demonstrated by the helical wheel representation, generated using DrawCoil 1.0 (*http://www.grigoryanlab.org/drawcoil*). (c) Mutations were introduced into the linker domain of MifS. The wild-type *mifS* gene or one of the mutated *mifS* genes were introduced into *E. coli* cells harbouring the *mifR* gene and the P_{PA5530}::*lacZ* reporter. Cells were grown in LB media to an OD_{600} value of 0.3 and challenged with α-KG or no substrate. LacZ expression levels were measured 60 min post-induction. Data points represent mean values±the standard deviations (n=3). Analysis of variance was performed by using Dunnett's post-hoc test (α value of 0.05) to identify significant differences (P<0.0001; marked with an asterisk).

DISCUSSION

Two-component systems are widely used by bacteria to sense and respond to their environments [21, 23, 35–40]. Although much work has been done to understand the cellular targets of TCSs, the signals that activate these TCSs remain poorly understood. The sensor histidine kinases of TCSs are an indispensable tool for a bacterium such as *P. aeruginosa* that occupies a range of different environmental niches and needs to constantly monitor and respond to environmental changes for survival [41–45]. The metabolic versatility of *P. aeruginosa* is dependent on its ability to precisely detect specific metabolites in its environment and regulate gene expression accordingly [3, 15, 45–49]. Dicarboxylates are an important group of metabolites for *P. aeruginosa* [1–3]. This is evident in the fact that the *P. aeruginosa* PAO1 genome harbours genes for three TCSs for dicarboxylate sensing: DctB/DctD (C4-dicarboxylate sensor), MifS/MifR (α-KG sensor) and AauS/AauR (putative glutamate sensor), while most bacteria only possess one TCS for sensing dicarboxylates, namely the DctB/DctD TCS [3, 42, 45].

In this study, we have characterized the MifS histidine kinase of *P.* aeruginosa PAO1, the only characterized histidine kinase that responds to α-KG. The response of histidine kinases to C4-dicarboxylates have been well documented [10, 11, 50–52]. Although sequence analysis suggests that MifS is a homologue of DctB (Fig. 1b), our data show that, unlike DctB, which is activated by several C4-dicarboxylates [10, 45], MifS only responds with high specificity to the C5-dicarboxylate α-KG (Fig. 2).

The sensor domains of dicarboxylate-sensing histidine kinases such as DctB, DcuS and CitA have been shown to adopt the PDC fold, an α/β mixed fold [10, 12]. Our model predicts that the MifS periplasmic sensor domain also adopts a PDC fold. DcuS and CitA, the first dicarboxylate sensors crystalized, have one PDC folded domain [10, 12]. MifS, however, has a sensor domain that is almost twice the size of the CitA or DcuS. We found the MifS sensor domain is arranged in two tandem PDC subdomains with the substrate binding pocket located in the subdomain distal to the membrane (Fig. 3a). This arrangement was also seen in the *Vc*DctB sensor, which has a sensor domain that is comparable in size to MifS [10].

In addition to similar sizes and structures, the MifS and DctB sensor domains also share sequence homology (33% identity, 90% coverage). Structural alignment of the *Vc*DctB ligand binding pocket with that of MifS showed, interestingly, that many of the key residues within the DctB binding pocket are conserved within MifS (Fig. 7). In fact, several important MifS binding pocket residues we identified are conserved as identical residues in *Vc*DctB: R135A (R130 in DctB), Y137 (Y132 in DctB), S156 (S151 in DctB) and K181 (K175 in DctB). Our model and mutational analysis indicate that all these residues are involved in providing

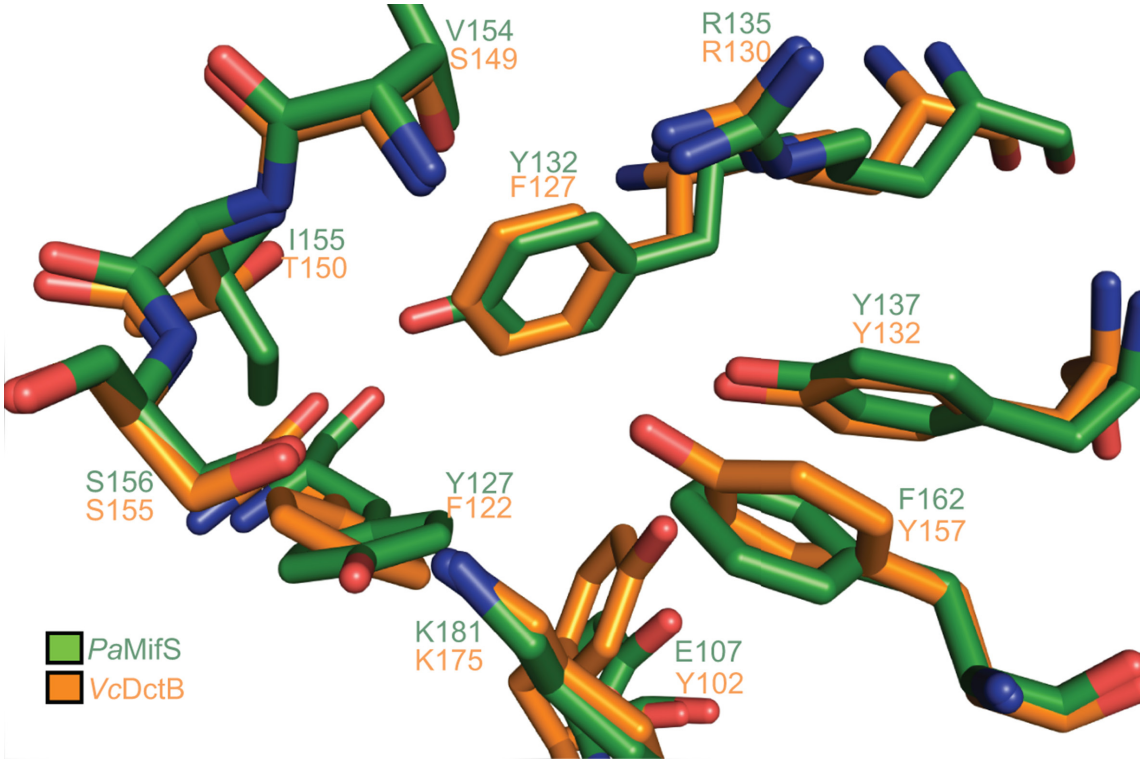

Fig. 7. MifS shares sequence and structural homology with DctB. A structural alignment of the MifS substrate binding pocket with that of *V. cholerae* DctB shows that the sensor domains of these two histidine kinases have several conserved residues. Structural alignment performed using PyMOL [19].

hydrogen bonds to the substrate in MifS, as has been shown for DctB.

So, why then does MifS respond to α-KG with such high specificity? We found that there are some subtle differences in the MifS and DctB binding pockets that may account for the different specificities of the two sensors. Differences in the size of the side-chains and available hydrogen bonds likely determine the identity of the substrate recognized by each histidine kinase. Our data show that a Tyr127 in MifS in place of the Phe122 in DctB contributes significantly to the α-KG response in MifS. Although this is a conserved substitution, a Y127F mutation significantly reduces the activity of MifS (Fig. 4). This suggests that the availability of the extra hydrogen bond due to the hydroxyl group of Tyr at this position is important for substrate specificity in MifS. So, the addition of one hydroxyl group through the substitution of a Tyr for a Phe significantly changes the substrate specificity. An example of an unfavourable effect of an extra hydroxyl on α-KG specificity is demonstrated by the F162 residue of MifS, which takes the place of Y157 in DctB that has been shown to be involved in hydrogen bonding with succinate [10]. We found that the F162 residue is required for sensing α-KG, and an F162Y mutation displayed significantly reduced activity (Fig. 4). The extra hydroxyl group in Tyr could lead to an unwanted interaction with α-KG and affect the size of the binding pocket. In this case, it appears that lack of the hydroxyl group helps MifS accommodate the longer substrate α-KG.

One notable difference in the MifS binding pocket is the presence of a Glu residue at position 107. All DctB homologues have a highly conserved Tyr or Phe at this position (Fig. 5a). The DctB structure does not show any involvement of this Tyr residue in substrate binding [10]. However, we found that E107 is important for α-KG response in MifS (Fig. 4). Both the E017A and E107Y mutations significantly reduced the activity of MifS (Fig. 4). Although our model predicts no direct interaction of E107 with α-KG (Fig. 3b), it is possible that this residue determines the size of the dicarboxylate in the pocket.

Overall, we identified five residues required for succinate binding in the *Vc*DctB sensor domain that were not fully conserved in MifS (Figs 5a and 7). We hypothesized that mutation of these residues in MifS to mimic DctB would increase succinate sensitivity in MifS. Indeed, mutation of Phe162 to a Tyr to resemble the *Vc*DctB Tyr157 increased succinate response while significantly reducing the α-KG response of MifS (Figs 4 and 5b). Interestingly, the F162Y mutation also significantly reduces the response of MifS to glutarate. From our modelling of the MifS binding domain, it appears that if there was a Tyr at position 162, the hydroxyl group would restrict the size of the binding

pocket, thus excluding the longer C5-dicarboxylates from entering, while allowing the shorter C4-dicarboxylate succinate to bind more efficiently to the pocket (Fig. 7). However, the F162Y mutation did not enhance the MifS response to any other C4-dicarboxylates. Therefore, it is likely not just a matter of change in size of the pocket. Encouraged by this result, we went on to make further mutations in MifS to resemble DctB. None of the other mutations showed any increase in succinate sensitivity. It is possible that a combination of several mutations might be required for MifS to gain succinate sensitivity and lose α-KG sensitivity. So, while F162 may be involved in determining substrate specificity, further work needs to be done to characterize the determinants of MifS substrate specificity.

Our model of the MifS binding pocket also shows us a likely reason why MifS does not respond to glutarate as well as it does to α-KG. Our model shows that the carbonyl group of α-KG makes one important H-bond with a binding pocket residue (Fig. 3b). Since glutarate lacks a carbonyl group, this bond is missing and thus the affinity of MifS for glutarate is significantly reduced.

Although it is possible that change in activity observed for some of the binding pocket mutations could be due to negative effects on protein structure and folding, or on the expression of the *mifS* gene, our data suggest that mutations in the predicted binding pocket residues affect the function of MifS regardless of the mechanism and, thus, play an important role in MifS function. Further *in vitro* structure–function studies are required to elucidate the role each residue plays in ligand binding.

The sensor domain of MifS is followed by a cytoplasmic coiled-coil linker domain that we found to be important for signal transduction (Figs 1a and 6). Recent studies have identified cytoplasmic coiled-coil linker domains that function in propagating signals from the sensor to the transmitter domain in several histidine kinases, including AgrC of *Staphylococcus aureus* [53] and BvgS of *Bordotella pertussis* [54]. Coiled coils are usually left-handed amphipathic helices with the non-polar residues facing outwards and making a dimerization surface composed of heptads annotated 'abcdefg' [33, 34]. The residues at a and d positions are typically leucines, forming the surface of the coil, whereas the other residues are usually polar and induce coil formation. We analysed one predicted heptad of the MifS linker domain spanning from residue 336 to residue 342. Modelling and sequence analysis suggests that the Leu residues at positions a and d of this heptad face outwards and form the dimerization surface (Fig. 6b) and, hence, mutations in these residues affected α-KG response (Fig. 6c). The charged residues, however, are not involved in dimerization and therefore mutations in these residues did not affect α-KG response (Fig. 6). Interestingly, we found that the deletion of part of the coiled coil leads to constitutive activity of MifS. Coiled coils are capable of transmitting conformational changes along their length [34, 53, 54]. Deletion of part of the coiled coil likely changes the conformation so that the linker domain is always in the active conformation. Further studies will show whether this coiled-coil domain of MifS is involved in α-KG-induced dimerization.

In conclusion, our work here shows that MifS is the first characterized α-KG sensor histidine kinase. Our data reveal that MifS is a specific sensor of α-KG, even though it is a homologue of the DctB family of C4-dicarboxylate-sensing histidine kinases. This further exemplifies the diverse metabolic capabilities and the extensive signal transduction capabilities that the soil bacterium *P. aeruginosa* possesses.

Funding information
This study was funded by the NIH (2R15GM104880-03 to C. T. N. and B. R. L.). The funding agency had no role in study design, data collection and interpretation, or the decision to submit the work for publication.

Acknowledgements
We gratefully acknowledge support from the Undergraduate Honors Program of SUNY-ESF, the Center for Applied Microbiology at SUNY-ESF, CSTEP at SUNY-ESF and the SOSA program of TCNJ.

Conflicts of interest
The authors declare that there are no conflicts of interest.

References

1. Siegel LS, Hylemon PB, Phibbs PV. Cyclic adenosine 3',5'-monophosphate levels and activities of adenylate cyclase and cyclic adenosine 3',5'-monophosphate phosphodiesterase in *Pseudomonas* and *Bacteroides*. *J Bacteriol* 1977;129:87–96.
2. Collier DN, Hager PW, Phibbs PV. Catabolite repression control in the pseudomonads. *Res Microbiol* 1996;147:551–561.
3. Lundgren BR, Villegas-Peñaranda LR, Harris JR, Mottern AM, Dunn DM *et al*. Genetic analysis of the assimilation of C5-dicarboxylic acids in *Pseudomonas aeruginosa* PAO1. *J Bacteriol* 2014;196:2543–2551.
4. Mailloux RJ, Singh R, Brewer G, Auger C, Lemire J *et al*. Alpha-Ketoglutarate dehydrogenase and glutamate dehydrogenase work in tandem to modulate the antioxidant alpha-ketoglutarate during oxidative stress in *Pseudomonas fluorescens*. *J Bacteriol* 2009;191:3804–3810.
5. Lemire J, Milandu Y, Auger C, Bignucolo A, Appanna VP *et al*. Histidine is a source of the antioxidant, alpha-ketoglutarate, in *Pseudomonas fluorescens* challenged by oxidative stress. *FEMS Microbiol Lett* 2010;309:no–177.
6. Guo W, Cai L-L, Zou H-S, Ma W-X, Liu X-L *et al*. Ketoglutarate transport protein KgtP is secreted through the type III secretion system and contributes to virulence in *Xanthomonas oryzae* pv. oryzae. *Appl Environ Microbiol* 2012;78:5672–5681.
7. Cai W, Wannemuehler Y, Dell'anna G, Nicholson B, Barbieri NL *et al*. A novel two-component signaling system facilitates uropathogenic *Escherichia coli*'s ability to exploit abundant host metabolites. *PLoS Pathog* 2013;9:e1003428.
8. Stock AM, Robinson VL, Goudreau PN. Two-Component signal transduction. *Annu Rev Biochem* 2000;69:183–215.
9. Krell T, Lacal J, Busch A, Silva-Jiménez H, Guazzaroni M-E *et al*. Bacterial sensor kinases: diversity in the recognition of environmental signals. *Annu Rev Microbiol* 2010;64:539–559.
10. Cheung J, Hendrickson WA. Crystal structures of C4-dicarboxylate ligand complexes with sensor domains of histidine kinases DcuS and DctB. *J Biol Chem* 2008;283:30256–30265.
11. Pappalardo L, Janausch IG, Vijayan V, Zientz E, Junker J *et al*. The NMR structure of the sensory domain of the membranous two-component fumarate sensor (histidine protein kinase) DcuS of *Escherichia coli*. *J Biol Chem* 2003;278:39185–39188.

12. Sevvana M, Vijayan V, Zweckstetter M, Reinelt S, Madden DR *et al*. A ligand-induced switch in the periplasmic domain of sensor histidine kinase CitA. *J Mol Biol* 2008;377:512–523.
13. Zhang Z, Hendrickson WA. Structural characterization of the predominant family of histidine kinase sensor domains. *J Mol Biol* 2010;400:335–353.
14. Cheung J, Bingman CA, Reyngold M, Hendrickson WA, Waldburger CD. Crystal structure of a functional dimer of the PhoQ sensor domain. *J Biol Chem* 2008;283:13762–13770.
15. Sarwar Z, Lundgren BR, Grassa MT, Wang MX, Gribble M *et al*. GcsR, a TyrR-Like enhancer-binding protein, regulates expression of the glycine cleavage system in *Pseudomonas aeruginosa* PAO1. *mSphere* 2016;1.
16. Zhang X, Bremer H. Control of the *Escherichia coli* rrnB P1 promoter strength by ppGpp. *J Biol Chem* 1995;270:11181–11189.
17. Waterhouse A, Bertoni M, Bienert S, Studer G, Tauriello G *et al*. SWISS-MODEL: homology modelling of protein structures and complexes. *Nucleic Acids Res* 2018;46:W296–W303.
18. Trott O, Olson AJ. Autodock Vina: improving the speed and accuracy of docking with a new scoring function, efficient optimization, and multithreading. *J Comput Chem* 2010;31:455–461.
19. Schrödinger. Llc. The PyMOL molecular graphics system, version 1.8.
20. Stewart RC. Protein histidine kinases: assembly of active sites and their regulation in signaling pathways. *Curr Opin Microbiol* 2010;13:133–141.
21. Mascher T, Helmann JD, Unden G. Stimulus perception in bacterial signal-transducing histidine kinases. *Microbiol Mol Biol Rev* 2006;70:910–938.
22. Grebe TW, Stock JB. The Histidine Protein Kinase Superfamily. In: Poole RK (editor). *Advances in Microbial Physiology*. Academic Press. pp. 139–227.
23. Sarwar Z, Garza AG. The Nla6S protein of *Myxococcus xanthus* is the prototype for a new family of bacterial histidine kinases. *FEMS Microbiol Lett* 2012;335:86–94.
24. Karniol B, Vierstra RD. The HWE histidine kinases, a new family of bacterial two-component sensor kinases with potentially diverse roles in environmental signaling. *J Bacteriol* 2004;186:445–453.
25. Tatusov RL, Galperin MY, Natale DA, Koonin EV. The COG database: a tool for genome-scale analysis of protein functions and evolution. *Nucleic Acids Res* 2000;28:33–36.
26. Marchler-Bauer A, Bo Y, Han L, He J, Lanczycki CJ *et al*. CDD/SPARCLE: functional classification of proteins via subfamily domain architectures. *Nucleic Acids Res* 2017;45:D200–D203.
27. Tatke G, Kumari H, Silva-Herzog E, Ramirez L, Mathee K. *Pseudomonas aeruginosa* MifS-MifR Two-Component System Is Specific for α-Ketoglutarate Utilization. *PLoS One* 2015;10:e0129629.
28. Cheung J, Hendrickson WA. Sensor domains of two-component regulatory systems. *Curr Opin Microbiol* 2010;13:116–123.
29. Chakravarty S, Ung AR, Moore B, Shore J, Alshamrani M. A comprehensive analysis of Anion-Quadrupole interactions in protein structures. *Biochemistry* 2018;57:1852–1867.
30. Liu J, Yang J, Wen J, Yang Y, Wei X *et al*. Mutational analysis of dimeric linkers in peri- and cytoplasmic domains of histidine kinase DctB reveals their functional roles in signal transduction. *Open Biol* 2014;4:140023.
31. Crick FHC. Is alpha-keratin a coiled coil? *Nature* 1952;170:882–883.
32. Crick FHC. The packing of α-helices: simple coiled-coils. *Acta Crystallogr* 1953;6:689–697.
33. Truebestein L, Leonard TA. Coiled-Coils: the long and short of it. *Bioessays* 2016;38:903–916.
34. Mason JM, Arndt KM. Coiled coil domains: stability, specificity, and biological implications. *Chembiochem* 2004;5:170–176.
35. Lupas AN, Gruber M. The Structure of α-Helical Coiled Coils. In: *Advances in Protein Chemistry*. *Academic Press*pp.:37–38.
36. Abriata LA, Albanesi D, Dal Peraro M, de Mendoza D. Signal sensing and transduction by histidine kinases as unveiled through studies on a temperature sensor. *Acc Chem Res* 2017;50:1359–1366.
37. Sarwar Z, Garza AG. The Nla28S/Nla28 two-component signal transduction system regulates sporulation in *Myxococcus xanthus*. *J Bacteriol* 2012;194:4698–4708.
38. Skerker JM, Prasol MS, Perchuk BS, Biondi EG, Laub MT. Two-Component signal transduction pathways regulating growth and cell cycle progression in a bacterium: a system-level analysis. *PLoS Biol* 2005;3:e334.
39. McLoon AL, Kolodkin-Gal I, Rubinstein SM, Kolter R, Losick R. Spatial regulation of histidine kinases governing biofilm formation in *Bacillus subtilis*. *J Bacteriol* 2011;193:679–685.
40. Sarwar Z, Garza AG. Two-component signal transduction systems that regulate the temporal and spatial expression of *Myxococcus xanthus* sporulation genes. *J Bacteriol* 2016;198:377–385.
41. Stover CK, Pham XQ, Erwin AL, Mizoguchi SD, Warrener P *et al*. Complete genome sequence of *Pseudomonas aeruginosa* PAO1, an opportunistic pathogen. *Nature* 2000;406:959–964.
42. Winsor GL, Lam DKW, Fleming L, Lo R, Whiteside MD *et al*. Pseudomonas genome database: improved comparative analysis and population genomics capability for *Pseudomonas* genomes. *Nucleic Acids Res* 2011;39:D596–D600.
43. Goodman AL, Merighi M, Hyodo M, Ventre I, Filloux A *et al*. Direct interaction between sensor kinase proteins mediates acute and chronic disease phenotypes in a bacterial pathogen. *Genes Dev* 2009;23:249–259.
44. Dasgupta N, Wolfgang MC, Goodman AL, Arora SK, Jyot J *et al*. A four-tiered transcriptional regulatory circuit controls flagellar biogenesis in *Pseudomonas aeruginosa*. *Mol Microbiol* 2003;50:809–824.
45. Valentini M, Storelli N, Lapouge K. Identification of C(4)-dicarboxylate transport systems in *Pseudomonas aeruginosa* PAO1. *J Bacteriol* 2011;193:4307–4316.
46. Lundgren BR, Thornton W, Dornan MH, Villegas-Peñaranda LR, Boddy CN *et al*. Gene *PA2449* is essential for glycine metabolism and pyocyanin biosynthesis in *Pseudomonas aeruginosa* PAO1. *J Bacteriol* 2013;195:2087–2100.
47. Lundgren BR, Harris JR, Sarwar Z, Scheel RA, Nomura CT. The metabolism of (R)-3-hydroxybutyrate is regulated by the enhancer-binding protein PA2005 and the alternative sigma factor RpoN in *Pseudomonas aeruginosa* PAO1. *Microbiology* 2015;161:2232–2242.
48. Lundgren BR, Sarwar Z, Pinto A, Ganley JG, Nomura CT. Ethanolamine catabolism in *Pseudomonas aeruginosa* PAO1 is regulated by the enhancer-binding protein EatR (PA4021) and the alternative sigma factor rpoN. *J Bacteriol* 2016;198:2318–2329.
49. Lundgren BR, Sarwar Z, Feldman KS, Shoytush JM, Nomura CT. SfnR2 Regulates Dimethyl Sulfide-Related Utilization in *Pseudomonas aeruginosa* PAO1. *J Bacteriol* 2019;201:e00606–00618.
50. Janausch IG, Garcia-Moreno I, Unden G. Function of DcuS from *Escherichia coli* as a fumarate-stimulated histidine protein kinase in vitro. *J Biol Chem* 2002;277:39809–39814.
51. Golby P, Davies S, Kelly DJ, Guest JR, Andrews SC. Identification and Characterization of a Two-Component Sensor-Kinase and Response-Regulator System (DcuS-DcuR) Controlling Gene Expression in Response to C4-Dicarboxylates in *Escherichia coli*. *J Bacteriol* 1999;181:1238–1248.
52. Graf S, Schmieden D, Tschauner K, Hunke S, Unden G. The Sensor Kinase DctS Forms a Tripartite Sensor Unit with DctB and DctA for Sensing C4-Dicarboxylates in *Bacillus subtilis*. *J Bacteriol* 2014;196:1084–1093.
53. Wang B, Zhao A, Novick RP, Muir TW. Activation and inhibition of the receptor histidine kinase AgrC occurs through opposite helical transduction motions. *Mol Cell* 2014;53:929–940.
54. Lesne E, Krammer E-M, Dupre E, Locht C, Lensink MF *et al*. Balance between coiled-coil stability and dynamics regulates activity of BvgS sensor kinase in *Bordetella*. *mBio* 2016;7:e02089.

55. **Kovach ME**, **Elzer PH**, **Hill DS**, **Robertson GT**, **Farris MA** *et al*. Four new derivatives of the broad-host-range cloning vector pBBR1MCS, carrying different antibiotic-resistance cassettes. *Gene* 1995;166:175–176.
56. **Madeira F**, **Park YM**, **Lee J**, **Buso N**, **Gur T** *et al*. The EMBL-EBI search and sequence analysis tools Apis in 2019. *Nucleic Acids Res* 2019;47:W636–W641.
57. **Robert X**, **Gouet P**. Deciphering key features in protein structures with the new ENDscript server. *Nucleic Acids Res* 2014;42:W320–W324.

Edited by: D. Grainger and M. Welch